THE JOURNAL OF PHYSICAL CHEMISTRY C

Article

pubs.acs.org/JPCC

High-Performance Supercapacitor Based on Three-Dimensional Hierarchical rGO/Nickel Cobaltite Nanostructures as Electrode Materials

Chuan Yi Foo,[†] Hong Ngee Lim,[*,†,‡] Mohd Adzir b. Mahdi,[§] Kwok Feng Chong,[∥] and Nay Ming Huang[⊥]

[†]Department of Chemistry, Faculty of Science, Universiti Putra Malaysia, 43400 UPM Serdang, Selangor Darul Ehsan, Malaysia

[‡]Functional Device Laboratory, Institute of Advance Technology, Universiti Putra Malaysia, 43400 UPM Serdang, Selangor Darul Ehsan, Malaysia

[§]Wireless and Photonics Network Research Centre, Faculty of Engineering, Universiti Putra Malaysia, 43400 UPM Serdang, Selangor Darul Ehsan, Malaysia

[∥]Faculty of Industrial Science & Technology, University Malaysia Pahang, Lebuhraya tun Razak, 26300 Gambang, Kuantan, Pahang Darul Makmur, Malaysia

[⊥]Centre of Printable Electronics, Deputy Vice Chancellor Office (Research & Innovation), University of Malaya, 50603 Kuala Lumpur, Malaysia

Supporting Information

ABSTRACT: A hybrid supercapacitor that employs nanomaterial has been extensively studied recently. However, inexorable collapse and agglomeration of metal oxide and short cycle stability of graphene sheets greatly hinder their practical applications. Herein, we demonstrate a competent synergic effect between nickel cobaltite (NCO) and reduced graphene oxide (rGO) for synthesizing the three-dimensional hierarchical rGO/NCO nanostructures via a facile one-pot hydrothermal method, followed by subsequent annealing in air. The structural and morphological characteristics of as-synthesized rGO/NCO have been characterized in-depth by FESEM, XRD, XPS, BET, and Raman spectroscopy. When incorporated in a two-electrode system with 2.0 M KOH electrolyte, the three-dimensional rGO/NCO nanostructures exhibit excellent supercapacitive performance. This is due to the unique properties of rGO that provide a flexible and expandable platform for growing NCO nanocrystals, which result in a nanoscopic rose petals morphology. These nanostructures provide a large surface area which facilitates the ion diffusion and eventually enhances the specific capacitance. Furthermore, performance studies between the as-synthesized electrode materials with a commercialized supercapacitor proved that the as-synthesized rGO/NCO electrode possesses a proficient potential to be a supercapacitor material, which provides high energy density as well as power density. A two-electrode system is advantageous over a conventional three-electrode system because it mimics the cell configuration of commercial supercapacitors.

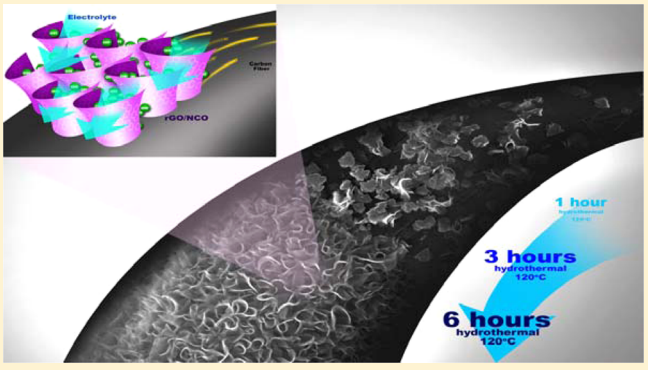

INTRODUCTION

In conjunction with the fast-growing market for developing hybrid electric vehicles and portable electronic devices, a high-power energy storage plays an important role in fulfilling the urgent demand for a sustainable energy system. An efficient energy storage device should possess high energy density that can be discharged instantly upon demand. Although rechargeable lithium-ion batteries can provide extremely high energy density, they typically required minutes to hours to discharge, not seconds. Besides that, these rechargeable batteries tend to require frequent replacement due to their electrochemical behavior and create environmental issues in addition to increasing lifecycle cost.[1−4] In order to enhance the charge/discharge rate of the energy storage devices, a supercapacitor was introduced to store the energy by means of a static charge as opposed to an electrochemical reaction which occurs in the batteries system. In other words, a supercapacitor that is able to store as much energy as a battery in minutes would be considered a groundbreaking achievement in today's energy storage technologies.

A supercapacitor (also known as a ultracapacitor or electrochemical capacitor)[5,6] is extensively used as backup energy storage which overcomes the deficiencies of other power sources, such as fuel cells and batteries, due to its pulse power

Received: June 12, 2016
Revised: August 12, 2016

© XXXX American Chemical Society

DOI: 10.1021/acs.jpcc.6b05930
J. Phys. Chem. C XXXX, XXX, XXX−XXX

supply, excellent cycle stability, and ability to charge and discharge rapidly at high power density.[5−7] Generally, on the basis of charge storage mechanism, a supercapacitor can mainly be classified into an electrical double layer capacitor (EDLC), which stores energy based on the accumulation of electrostatic charge at the electrode/electrolyte interface, and *pseudo*-capacitors, in which the energy stored based on the rapid surface redox reaction contributes by the electroactive species.[8,9] In this regard, both of the mechanisms can operate simultaneously in a hybrid system depending on the nature of electrode materials which are highly accessible to the electrolyte ions such as carbon nanotubes (CNTs), graphene and graphene derivatives, conductive polymers, and transition-metal oxides.[10−12]

On the basis of the relationship between the diffusion rate of electrolyte ions and their diffusion length,[2] the reduced characteristic dimensions of the electrode material (from microstructure to nanostructure particles) act as a key component in providing a superior supercapacitor performance.[13] In this case, nanostructure materials such as nanotubes, nanowires, nanosheets, and nanospheres have sparked huge interest in research activities to enhance supercapacitance effects. This is due to their small, porous structure which can provide a short ion transport pathway and high exposure to abundant active sites. Thus far, various kinds of transition-metal oxides have drawn extensive research attention in recent years as electrode materials. Among them, spinel nickel cobaltite (NCO), is an economic, environmentally friendly and easily synthesized transition-metal oxide, which has been employed in various kinds of *pseudo*-capacitive materials.[14] The unique core/shell $NiCo_2O_4$@$NiCo_2O_4$ structure has been reported as a low-cost and facile electrode material which provides excellent electrochemical performance in both supercapacitors and lithium-ion batteries.[15] Transition-metal oxide tends to give poor cycling performance due to the strain caused during charge/discharge cycles. Hence, to overcome this issue, nanostructured NCO with diverse morphologies can provide a better accommodation of the strain during ion transfer as compared to other microstructure materials. Although nanostructured NCO is feasible for superior supercapacitive properties, the nature of nanostructure materials which will self-assemble into large bulk owing to the high interface energy is restricting their practical applications.[14]

Generally, through combination of highly conductive backing with nanostructure materials, it can prevent the self-assemble issue and, at the same time, enhance their electrical conductivities and ion mobility.[9,16] A two-dimensional network material called graphene has become an attractive substrate for supercapacitor materials in the past decades due to its excellent mechanical properties and high conductivity, and most importantly, it can provide a large surface area and is easily obtained through simple chemical processing of graphite.[17,18] With the help of this virtue, various kinds of graphene−metal oxide nanocomposites have been widely reported for electrochemical storage.[19−23] The results show that, through the incorporation of graphene sheets into the transition-metal oxide system, it can provide an intimate integration between the nanostructure materials and the substrate, which can eventually prevent agglomeration and self-assemble.[24,25] Besides that, graphene sheets also offer a proficient electron transport pathway which facilitates the ion mobility and diffusion rate.[26,27] Graphene is also a very popular and ideal EDLC material which has been utilized in various kinds of supercapacitor applications.[28−30] Recently, a graphene derivative such as graphene oxide (GO) and reduced graphene oxide (rGO) has been extensively used in supercapacitor electrode material due to the presence of oxide functional groups. These oxide functional groups not only provide a high degree of monolayer architecture but also provide a better interaction with the metal oxide through the formation of M−O bonds (M = metal).[31,32]

By taking the advantages of each merit, a high-performance symmetrical supercapacitor by integrating the synergic effect between NCO and reduced graphene oxide (rGO) is demonstrated. rGO sheets are employed in designing the supercapacitor as an excellent backing material to anchor the NCO on the substrate and also prevent self-agglomeration. On top of that, the unique morphology of the as-synthesized product possesses numerous open spaces and surface area, providing a high specific reactive area and superior rate performance. The synthesized graphene decorated nickel cobaltite (rGO/NCO) nanostructures provide better anchoring properties toward the substrate and faster ionic transport compared to the pure NCO.

EXPERIMENTAL SECTION

Materials. Graphite powder was purchased from Ashbury Graphite Mills Inc., United States (code no. 3061). Phosphoric acid (H_3PO_4, 85%), sulfuric acid (H_2SO_4, 95−98%), charcoal activated powder (Chem-Pur), hydrogen peroxide (H_2O_2, 30%), potassium permanganate ($KMnO_4$, 99%), acetone (C_3H_6O), ethyl alcohol (C_2H_6O), and hydrochloric acid (HCl, 37%) were purchased from System, Malaysia. Nickel nitrate ($Ni(NO_3)_2{\cdot}6H_2O$), cobalt nitrate ($Co(NO_3)_2{\cdot}6H_2O$), and urea (CH_4N_2O) were purchased from Merk, Germany, and potassium hydroxide (KOH) was obtained from Fluka. The carbon cloth ELAT was purchased from NuVant, USA, and 55 mm qualitative filter paper was purchased from Advantec, Toyo Roshi Kaisha, Ltd., Japan. Double distilled water was used throughout the experiment.

Synthesis of Reduced Graphene Oxide/Nickel Cobaltite Nanostructures on Carbon Cloth. All chemicals were of analytical grade and used directly after purchase without any further purification. Before the deposition process, commercial carbon cloths with dimensions of 2 × 4 cm were cleaned by ultrasonication sequentially in 1.0 M HCl solution, acetone, distilled water, and ethyl alcohol for 15 min each. The washed carbon cloth was dried at room temperature and ready to use. Graphene decorated nickel cobaltite nanostructures arrays (rGO/NCO) on carbon cloth were synthesized through a facile one-pot hydrothermal method. 4 M $Ni(NO_3)_2{\cdot}6H_2O$ and 8 M $Co(NO_3)_2{\cdot}6H_2O$ were dissolved in distilled water, followed by the addition of 15 M urea at room temperature under continuous stirring to form a clear pink solution. 0.03 mg mL^{-1} of GO that was synthesized via a modified Hummer's method[33] was added into the mixture solution to form a total of 100 mL of a dark pink solution, followed by 30 min of ultrasonication. Then, the mixture was transferred into a 50 mL Teflon-lined stainless steel autoclave. The well-cleaned carbon cloth was immersed in the mixture, and the autoclave was kept at 120 °C for 6 h. After that, the autoclave was allowed to cool, and the product supported carbon cloth was washed with ethyl alcohol and ultrasonicated for 5 min to remove the loosely attached product on the surface. Lastly, the sample was dried and annealed at 400 °C for 2 h. The prepared samples were labeled as rGO/NCO. For comparison, pure NCO was

DOI: 10.1021/acs.jpcc.6b05930
J. Phys. Chem. C XXXX, XXX, XXX−XXX

Scheme 1. Schematic Illustration of Synthesis Process for Hierarchical rGO/NCO Nanostructures

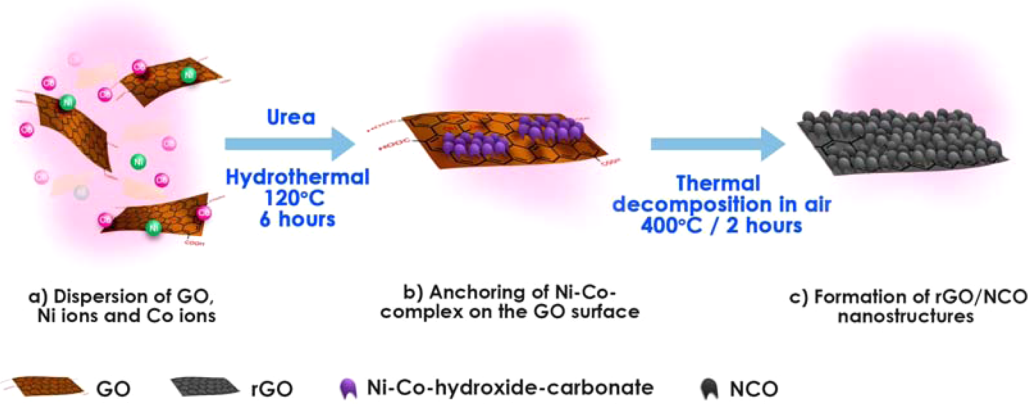

synthesized under the same hydrothermal method in the absence of GO.

Characterization of Reduced Graphene Oxide/Nickel Cobaltite Nanostructures. *Morphological and Structural Characterizations.* The crystalline structure of the products was identified by an X-ray diffraction (XRD) analysis using a D8 Advance (Bruker, Karlsruhe, Germany) automated X-ray diffractometer system with Cu−Kα radiation at 40 kV and 40 mA ranging from 10° to 80° at room temperature. The surface morphologies were analyzed using a field emission scanning electron microscope (FEI Quanta SEM Model 400F) equipped with an energy-dispersive X-ray (EDX) accessory. Raman spectra were carried out using a WITec Raman spectrophotometer (Alpha 300R). X-ray photoelectron spectroscopy (XPS) measurements were carried out on a scanning X-ray microprobe PHI Quantera II (Ulvac-PHI, INC.) using a monochromatic Al−Kα ($h\nu$ = 1486.6 eV) X-ray source that operated at 25.6 W (beam diameter of 100 μm). Wide scan analysis was performed using a pass energy of 280 eV with 1 eV per step for determination of elemental chemical states, while narrow scan analysis was performed throughout the binding energy range of interest at a pass energy of 112 eV with 0.1 eV per step.

Electrode Preparation and Electrochemical Measurements. The product deposited carbon cloth was measured and cut into few square pieces with surface area of 1 cm^2. Then, the square pieces was immersed into the 2 M KOH electrolyte solution for several minutes together with the dielectric material. The dielectric material used is standard graded filter paper. Both square pieces of product deposited carbon cloths were used for electrochemical measurement studies.

Electrochemical measurements were carried out by a Princeton potentiostat/galvanostat controlled by Versa Studio software. A two-electrode cell system was used to measure the electrochemical performance of the as-assembled symmetrical supercapacitor in 2 M KOH electrolyte with a filter paper as dielectric material. Both rGO/NCO nanostructures deposited carbon cloths (1 cm^2 each) were used as the positive and negative terminals, and a dielectric material is then sandwiching between the two electrodes in a Swage lock cell configuration.

The electrochemical impedance spectrum (EIS) analyses were carried out in the frequency range from 0.01 Hz to 30 kHz at open circuit potential with an ac perturbation of 10 mV. The specific capacitance value (C_{sp}) was calculated from the galvanostatic discharge curve, using following equation

$$C_{sp} = \frac{I\Delta t}{m\Delta V}\ (\mathrm{F\ g^{-1}}) \tag{1}$$

where I is the constant discharge current (A), Δt indicates the discharging time for a half-discharge (s), m represents the mass of corresponding active material (g), and ΔV represents the potential range of a half-discharge (V). The energy density (E) of the symmetrical supercapacitor was calculated by the specific capacitance (C_{sp}) and cell voltage (V) according to the following equation:

$$E = \frac{1}{2}C_{sp}V^2\ (\mathrm{Wh\ kg^{-1}}) \tag{2}$$

The power density (P) of the symmetrical supercapacitor was calculated by the E and the discharging time (t) according to the following equation:

$$P = \frac{E}{t}\ (\mathrm{W\ kg^{-1}}) \tag{3}$$

A comparison between the as-synthesized electrode materials with a bare NCO electrode as well as commercial KEMEX, 0.1 F supercapacitor was carried out using the same electrochemical measurement.

RESULTS AND DISCUSSION

Structural Properties and Morphologies of Reduced Graphene Oxide/Nickel Cobaltite Nanostructures. A plausible synthesis mechanism of the three-dimensional rGO/NCO nanostructures is shown in Scheme 1. First, the modified Hummer's GO was dispersed in the stock solution of Ni and Co precursor (Scheme 1a). The hydrophilic oxygen functional groups such as hydroxyl, carbonyl, carboxyl, and epoxy groups on the surface of GO provide excellent anchoring sites for positively charged Co^{2+} and Ni^{2+} ions through electrostatic forces, forming the Ni-Co complex (Scheme 1b).[11,34] Under the hydrothermal conditions at 120 °C, NCO nanocrystals were formed on the surface of the GO cluster through nucleation, an aggregative growth process, and a oriented attachment mechanism, simultaneously reducing GO to rGO. During these processes, the flexible properties of GO provide an expandable platform for the NCO crystal growth, which eventually turns into a nanoscopic rose petal morphology. The thermal treatment at 400 °C in air further removes the impurities on the nanocomposite (Scheme 1c).The synergic effect between the supporting rGO nanosheets and NCO nanocrystal provides apparent advantages for electrochemical

DOI: 10.1021/acs.jpcc.6b05930
J. Phys. Chem. C XXXX, XXX, XXX−XXX

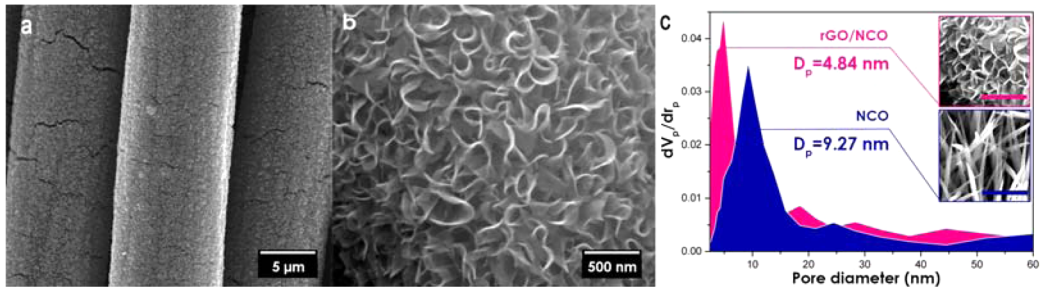

Figure 1. FESEM images of rGO/NCO nanostructure at (a) low and (b) high magnifications. (c) BET pore size distribution profiles, in correspondence to the insets. The scale bars in the insets are 600 nm.

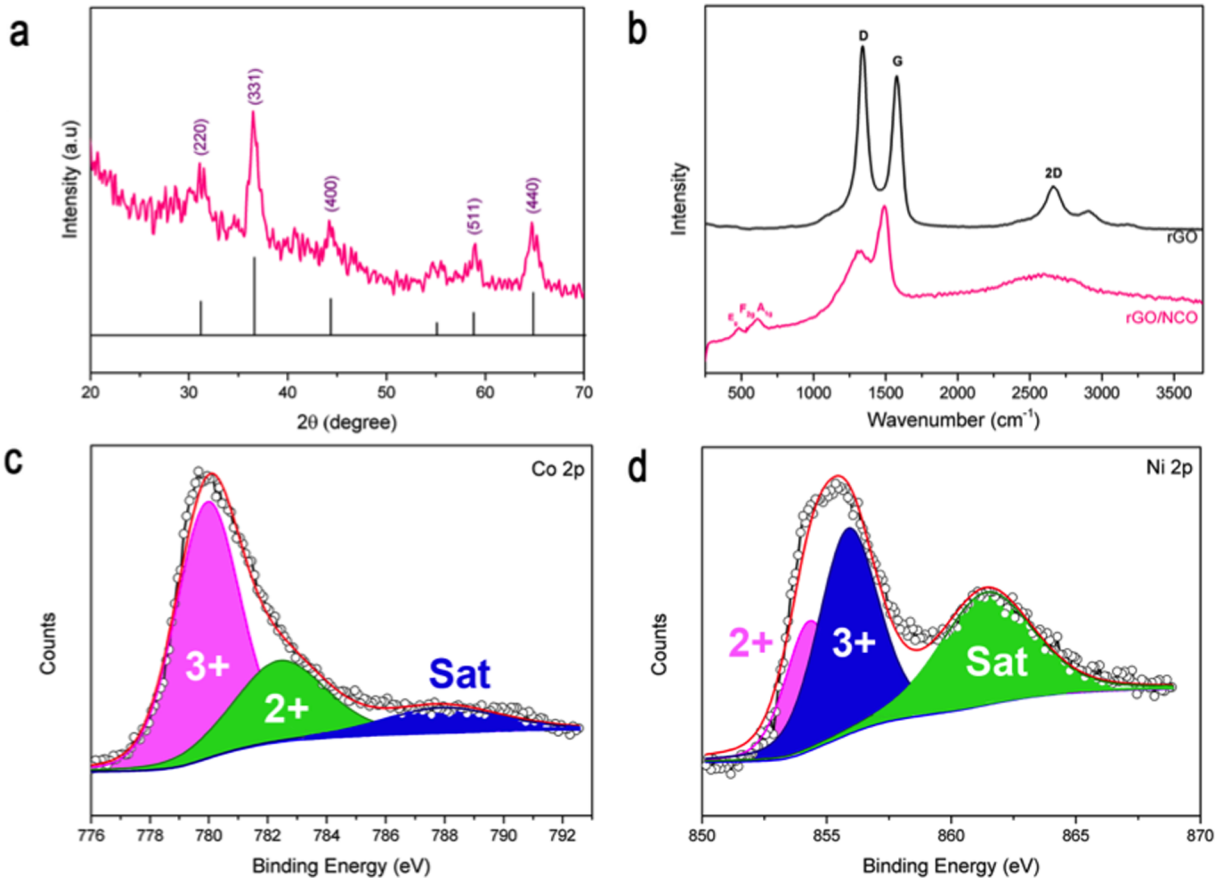

Figure 2. (a) XRD-pattern, (b) Raman spectrum, and high-resolution XPS spectra of (c) Ni 2p and (d) Co 2p of as-synthesized rGO/NCO nanostructures.

applications such as excellent capacitive activity and prolonged lifespan, which is discussed in the following paragraphs.

The morphology of the as-synthesized hierarchical rGO/NCO nanostructures observed using an FESEM at a low magification reveals a uniform distribution of nanocomposites on the carbon cloth (Figure 1a). There is no aggregation or agglomeration of nanostructures on the carbon cloth substrate, which indicates that the presence of rGO provides a platform for crystallization of NCO and an efficient contact between the NCO nanocrystal and the carbon cloth substrate. In contrast, the neat NCO nanoneedles deposited on a carbon cloth have micron-sized irregular speckles on them (Figure S1). Figure 1b shows a high magnification of the nanosized three-dimensional configuration that is constructed by randomly oriented rose-petal-like units. More importantly, the rose-petal-like morphology resulted in a high Brunauer–Emmett–Teller (BET) specific surface area of 105.1 m^2 g^{-1}, which is 2 times higher than that of the neat NCO owing to that the as-synthesized rGO/NCO nanostructures possess abundant open space and sufficient electrode/electrolyte interface for electrochemical reaction (Figure S2). Moreover, the corresponding pore size distribution data in Figure 1c show that the average diameter of the mesopores is 4.84 nm for rGO/NCO nanostructures and 9.27 nm for neat NCO nanoneedles. The inset of Figure 1c clearly depicts that the sizes of the mesopores in the neat NCO nanoneedles are apparently larger than those of the rGO/NCO nanostructures. The generation of these mesopores in both rGO/NCO nanostructures and pure NCO nanoneedles can be ascribed to the release of CO_2 and H_2O using the thermal decomposition of the Ni-Co complex.

The crystallographic structure of rGO/NCO is further inspected through X-ray diffraction (XRD). By comparing the

DOI: 10.1021/acs.jpcc.6b05930
J. Phys. Chem. C XXXX, XXX, XXX−XXX

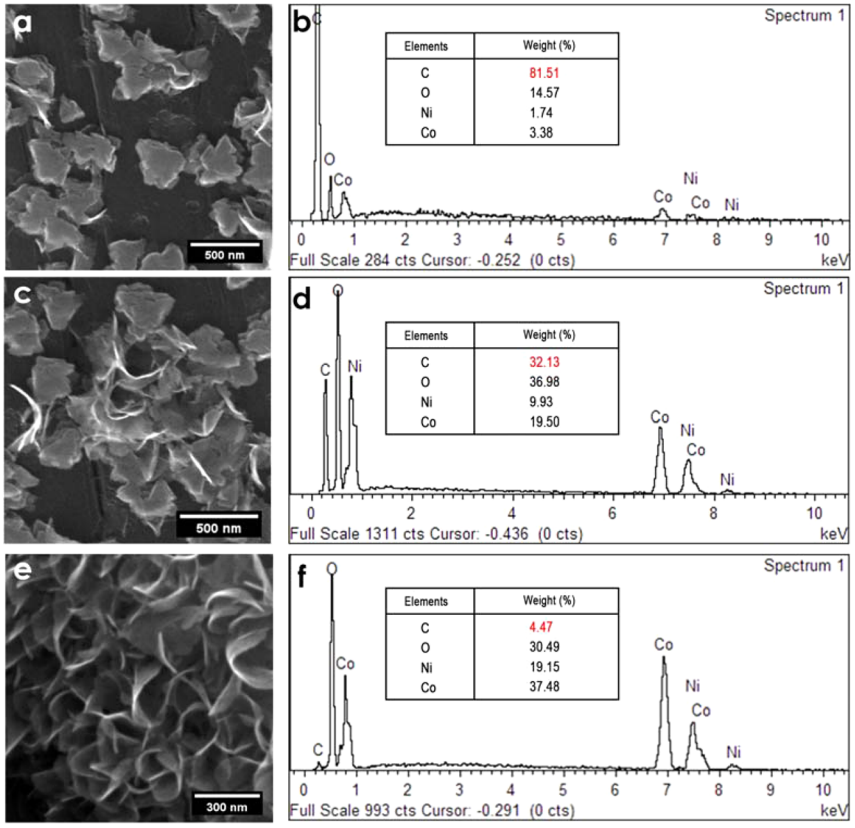

Figure 3. Representative FESEM images of samples obtained after reaction times of (a) 1 h, (c) 3 h, and (e) 6 h. Panels (b), (c), and (f) are the corresponding EDX analysis results for the formation process for the hierarchical rGO/NCO nanostructures.

XRD pattern of both product before and after calcination, it can be confirmed that the Ni-Co complex synthesized from the hydrothermal method is converted into spinel nickel cobaltite through thermal decomposition at 400 °C (Figure S3). Although the intensity of the diffraction peak is fairly weak due to the ultrathin architecture, the (220), (331), (400), (511), and (440) peaks in the diffractogram (Figure 2a) can be satisfactorily assigned to the cubic nickel cobaltite ($NiCo_2O_4$) phase. The exfoliated rGO in the synthesis routine causes no significant peak being observed from the XRD pattern; however, the existence of rGO is revealed in the Raman analysis. As seen in Figure 2b, the peaks at 462, 505, and 667 cm^{-1} correspond to E_g, F_{2g}, and A_{1g} modes of NCO, respectively. In addition, two significant peaks at 1342.66 and 1576.68 cm^{-1} were observed, attributed to the D band and G band of the rGO nanosheets array.[35,36] It can be clearly seen that the D and G bands in the synthesized electrode got shifted to lower wavenumber (1283.81 and 1489.44 cm^{-1}, respectively), revealing that there is an increase in the surface defect of the rGO that was induced during the synthesis process, which was attributed to the deposition of NCO nanocrystal on top of the rGO surface. The further confirmation of the existence of both Ni and Co elements within the as-prepared rGO/NCO nanostructures is shown in X-ray photoelectron (XPS) measurements, which provide a more comprehensive information regarding their oxidation states (Figure S4). Narrow scan of the spectra (Figure 2c,d) reveals that the presence of Ni^{2+}/Ni^{3+} and Co^{2+}/Co^{3+} cations is well fitted into the Gaussian fitting method, and the shakeup satellites are denoted as "Sat.".

It is noteworthy that the formation of hierarchical rGO/NCO nanostructures is vital to the capacitive performance of the electrode material. Therefore, time-dependent experiments have been carried out to gain a better insight regarding the evolution process of Ni and Co precursors. As delineated in Figure 3a, the smooth carbon fibers surface is scattered by numerous clusters of nanostructures at the beginning of the hydrothermal reaction. In addition, the increased *C* intensity observed in the EDX spectrum (Figure 3b) and the emergence of a thin layer at the edge of these nanocluster clearly demonstrate the GO nature of the cluster products. However, these nanoclusters are not thermodynamically stable over a period of time. When the reaction time is extended to 3 h, some thin and small nanosheets start to emerge around the surface of the nanocluster (Figure 3c). With the progression of the hydrothermal reaction, the sheets continue to propagate and a significant increase in the Ni and Co peaks can be observed in the EDX spectrum (Figure 3d), as the nanocrystals started to grow and expand on the flexible GO nanosheet. At the final stage of the reaction, the fully expanded nanoclusters evolve into a rose-petal-like nanoarchitecture (Figure 3e) with NCO crystals deposited on top of the GO sheets. During the continuous hydrothermal process, the compositional change is validated by the EDX spectrum. The emergence of the rose-petal-like morphology corresponds with the evolving characteristic peaks of Ni and Co. As the reaction time progresses, these two peaks become dominant and eventually overtake the C peak (Figure 3f). Moreover, the Ni/Co ratio in the as-synthesized product is around 0.511, approaching the theoretical value of nickel cobaltite.

Electrochemical Capacitive Properties of Reduced Graphene Oxide/Nickel Cobaltite Nanostructure. Cyclic voltammetry (CV), galvanostatic charge/discharge (GCD), and

DOI: 10.1021/acs.jpcc.6b05930
J. Phys. Chem. C XXXX, XXX, XXX−XXX

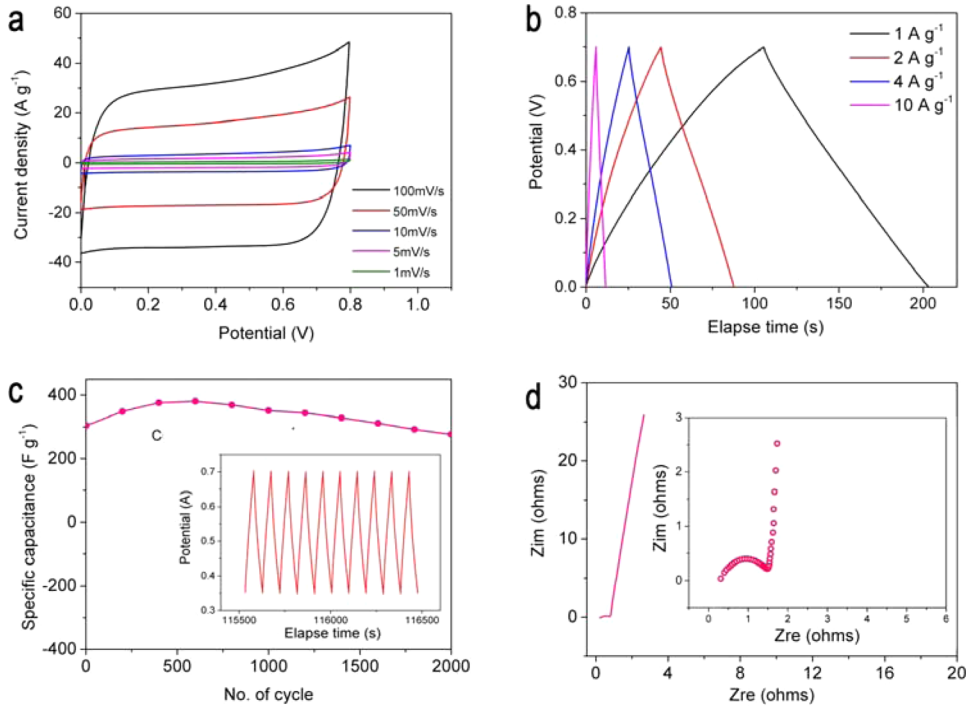

Figure 4. Electrochemical characterizations of as-synthesized rGO/NCO electrode. (a) CV curves, (b) GCD curves, (c) cycling stability at current density of 1 A g^{-1}, and (d) EIS spectrum. The inset in (c) shows the corresponding GDC curve for the last 10 cycles of the stability study, and the inset in (d) shows the high frequency region of the EIS spectrum.

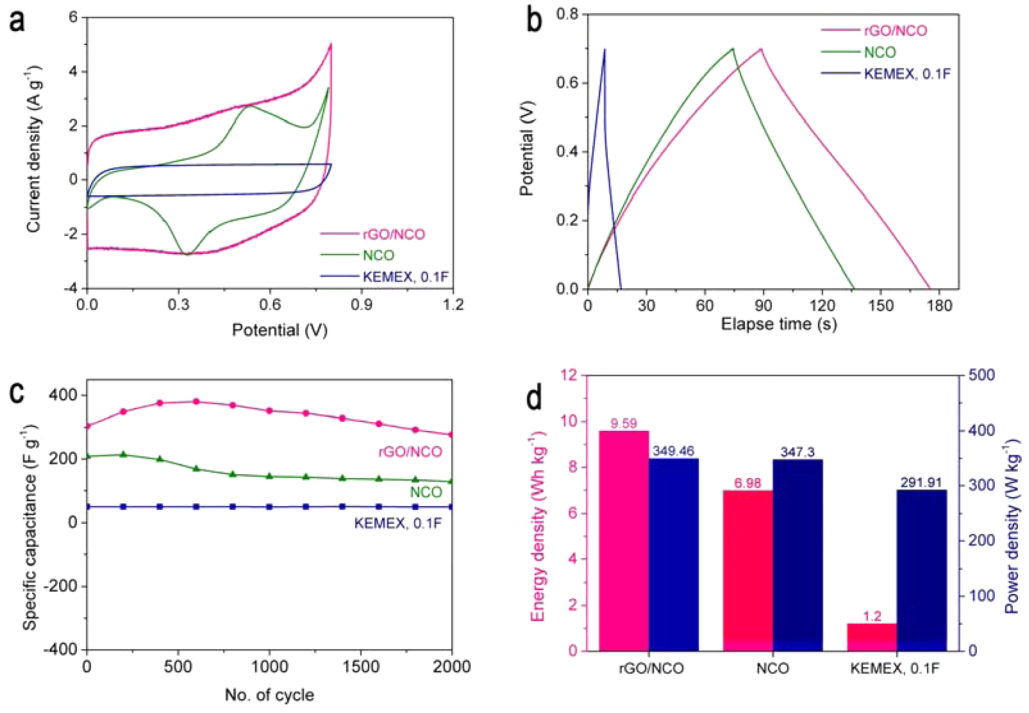

Figure 5. Comparison of rGO/NCO electrode against neat NCO electrode and commercial KEMEX 0.1 F supercapacitor. (a) CV curves at a constant scan rate of 10 mV s^{-1}, (b) GCD curves at a current density of 1 A g^{-1}, (c) cyclic stability after 2000 continuous charge/discharge cycles, and (d) energy and power densities.

electrochemical impedance spectroscopy (EIS) are employed to inspect the electrochemical capacitive performance of the three-dimensional rGO/NCO nanostructures as electrode for supercapacitor. CV analyses are characterized in a two-electrode system with 2.0 M KOH solution as the electrolyte at the various scan rates from 0 to 0.8 V. Figure 4a shows the typical CV curves of the rGO/NCO electrode that were obtained with different scan rates ranging from 1 to 100 mV s^{-1}. The CV curve observed in the rGO/NCO electrode is apparently more rectangular compared to that of the pure NCO (Figure S5), which indicates that the capacitive characteristic of the as-synthesized electrode materials is enhanced by the EDLC

DOI: 10.1021/acs.jpcc.6b05930
J. Phys. Chem. C XXXX, XXX, XXX−XXX

Table 1. Comparison of Electrochemical Performances of Hierarchical rGO/NCO Nanostructures with Other Representative Nickel Cobaltite Nanostructures

nickel cobaltite based nanostructures	specific capacitance in three-electrode system (F g^{-1})	specific capacitance in two-electrode system (F g^{-1})	stability	ref
nickel cobaltite double-shell hollow sphere	568 (1 A g^{-1})	not reported	85.8%, 2000 cycles	38
CNT/nickel cobaltite core shell	695 (1 A g^{-1})	not reported	91.0%, 1500 cycles	39
ultrathin nickel cobaltite nanosheet	1472 (1 A g^{-1})	not reported	99.0%, 3000 cycles	40
nickel cobaltite on nitrogen doped graphene sheet	508 (0.5 A g^{-1})	not reported	93.0%, 2000 cycles	41
rGO/nickel cobaltite nanostructures	613 (1 A g^{-1})	282.94 (1 A g^{-1})	90.9%, 2000 cycles	this work

properties of the rGO nanosheets. Besides that, the integral area of CV curves of the rGO/NCO electrode is substantially greater than that of pure NCO because the pure NCO nanoparticles aggregate easily and provide poor capacitive performances in the two-electrode system. Figure 4b shows the GCD curves of the rGO/NCO electrode at a current density of 1, 2, 4, and 10 A g^{-1}. The specific capacitance of the electrode material is indicated through the discharging period; the longer the discharging time, the better the specific capacitance. As calculated from eq 1, the specific capacitances corresponding to the current densities are 282.94, 262.80, 258.89, and 214.21 F g^{-1}, respectively. This indicates that around 76% of capacitance was retained when the charge−discharge density increased from 1 to 10 A g^{-1}. Importantly, the long-term cycling performance is very stable after continuous cycling for 2000 charge−discharge cycles with a specific capacitance of 276.76 F g^{-1} (Figure 4c). The increment of the capacitance in the beginning of the life cycle indicates the activation of the electrode, which allowed the ions to diffuse out slowly into the electrolyte. After the full activation of the electrode materials, the capacitance performance of the electrode decreases gradually as the cycle proceeds, which indicates that the degradation of the electrode materials occurs.[37] Overall, the capacitance retention is about 90.9% compared with the initial capacitance of the first cycle and the good cycle stability of the as-synthesized rGO/NCO nanostructures may be related to the feasible ionic transport at the electrode surface, which was further designated by the electrochemical impedance spectroscopy (EIS) measurement. The Nyquist plot of the rGO/NCO electrode in a frequency range of 0.1 Hz until 300 kHz in 2.0 M KOH electrolyte is shown in Figure 4d. A small semicircle region at the high frequency region indicates low charge transfer resistance at the electrode/electrolyte interface. In addition, the result also shows low diffusion resistance of the hierarchical product where the intercept of the arc on the *x*-axis is relatively close to zero. The steeper shape of the low frequency region represents an ideal capacitive behavior, indicating that the fast ion transport in the electrode is due to its large reactive surface area and intimate integration of electrode materials with the substrate.[38]

Performance Studies of the As-Synthesized Reduced Graphene Oxide/Nickel Cobaltite Electrode. The unique morphology of the as-synthesized rGO/NCO electrode makes it suitable for high capacity and long cycle stability energy storage. Unambiguously, the nanostructure of rGO/NCO consisting of numerous rose-petal-like arrays possesses a high surface area, thus providing a greatly reduced diffusion length, and various active sites for redox reaction to take place. In addition, the high surface area of the product ensures that most of the electroactive species are involved in the electrochemical charge storage mechanism, and thus efficiently contributes to the total capacitance.

For comparison, electrochemical performances of pure NCO and the commercial supercapacitor (KEMEX, 0.1 F) were evaluated. The representative CV curves at 10 mV s^{-1} in a potential window of 0−0.80 V are plotted in Figure 5a. A distinguishable typical rectangular shape with no distinctive redox peak can be observed for the KEMEX, 0.1 F supercapacitor, demonstrating the conventional EDL behavior of a carbon based supercapacitor. Meanwhile, a significant redox peak can be observed from the neat NCO and slightly noticeable on rGO/NCO electrodes, which indicates that reversible Faradaic reaction takes place in the charge storage mechanism. Interestingly, the areas under the curves of rGO/NCO and NCO are remarkably higher than that of the KEMEX, 0.1 F supercapacitor. This further proves that the presence of redox species in the two-electrode system can effectively harvest the electroactive species through the rapid reversible Faradaic reaction and thus provides extra charge for the storage mechanism. As shown in Figure 5b, the specific capacitances calculated from the GCD curves for the as-synthesized rGO/NCO electrode, the pure NCO electrode, and the KEMEX, 0.1 F supercapacitor are 282.95, 182.10, and 50.7 F g^{-1}, respectively. This indicates that the enhanced electrochemical behavior achieved by incorporating redox active species in the two-electrode system can provide a better charge/discharge performance compared to commercial carbon based EDLC (KEMEX, 0.1 F), yet the charge storage performance for the neat NCO electrode in the two-electrode system is inferior due to the agglomeration of the nanoneedles. On the other hand, the open spaces between the nanostructures act as a robust reservoir for electroactive species and also effectively enhance the diffusion kinetic within the electrode. More importantly, the intimate integration of NCO nanocrystals on the rGO nanosheet results in an efficient contact between the electrode/electrolyte interface, and thus a sufficient Faradaic reaction can occur even at very high current densities. The only drawback of the rGO/NCO electrode compared to the commercial KEMEX, 0.1 F supercapacitor is the long-term cycling stability (Figure 5c). Although the specific capacitance generated from the KEMEX, 0.1 F supercapacitor is much lower compared to the rGO/NCO electrode, the high capacitance retention (99.6%) can provide a stable and continuous supply in various electronic devices which operate in low power density. On the other hand, the capacitance retention of rGO/NCO nanostructures electrode is 90.9%, and it is more superior than the neat NCO by 46%. The presence of rGO in the spinel transition-metal oxide system withstands the strain relaxation and mechanical deformation,

DOI: 10.1021/acs.jpcc.6b05930
J. Phys. Chem. C XXXX, XXX, XXX−XXX

preventing the electrode materials from self-aggregating and slumping from the substrate surface. Taking these experimental results into consideration, the as-synthesized hierarchical rGO/NCO nanostructures are promising electrode material for a high-performance symmetrical supercapacitor which shows a comparable capacitive result with commercial carbon based EDLC. As shown in Figure 5d, the proposed electrode system can provide a significant high energy and power density (9.59 Wh kg^{-1} and 349.46 W kg^{-1}) compared to the neat NCO electrode (6.98 Wh kg^{-1} and 347.30 W kg^{-1}) as well as the KEMEX, 0.1 F supercapacitor (1.20 Wh kg^{-1} and 291.91 W kg^{-1}).

Unlike the widely reported supercapacitors in a three-electrode system, this work reported on a supercapacitor in a two-electrode system (Table 1). The incredibly high specific capacitance response from a three-electrode system is mainly credited to the unlimited access of free moving ions that are involved in a charge storage mechanism as the electrode material is exposed to an excess of electrolyte solution. However, a three-electrode cell configuration is impractical for commercial supercapacitor application because they are manufactured following a two-electrode configuration. A two-electrode configuration minimizes the use of electrolyte solution, consequently curtailing the leakage of the supercapacitor, and thus provides an economic fabrication of supercapacitors. Moreover, the superior electrochemical performance is merited to the synergic effects of two highly capacitive electrode materials, excellent ionic transport medium, and enhanced reactive surface area of the rGO/NCO rose-petal-like nanostructures.

CONCLUSION

In conclusion, we have developed a facile one-pot hydrothermal method to fabricate a three-dimensional hierarchical electrode material constructed by rGO/NCO nanostructures. Clusters of stacked GO sheets are initially formed during the hydrothermal reaction, which then evolved into a rose-petal-like nanostructure through nucleation and aggregative growth of the NCO nanocrystal. The as-synthesized Ni-Co complex is converted into rGO/NCO through hydrothermal and subsequent annealing in air. The final hierarchical rGO/NCO nanostructures manifest promising electrochemical properties as a *pseudo*-capacitive type electrode material for symmetrical supercapacitors with excellent capacitive performance and long cyclic stability. Overall, the as-synthesized rGO/NCO nanostructures show promising potential as an electrode material for high-performance supercapacitors. Furthermore, by comparing with a commercial carbon based supercapacitor, the rGO/NCO electrode shows better charge/discharge properties with higher specific capacitance. Although the capacitance retention is lower than that of the commercial supercapacitor, the rGO/NCO electrode provides remarkably high energy and power densities. This indicates that the proposed rGO/NCO nanostructures are a promising electrode material for high-performance supercapacitors. Furthermore, the integrative approach of designing electrode materials from this research is a vital reference to synthesize similar materials. The practical two-electrode configuration employed to measure the electrochemical performance of the synthesized electrode materials manifests plausible commercial use of the as-fabricated supercapacitor.

ASSOCIATED CONTENT

Supporting Information

The Supporting Information is available free of charge on the ACS Publications website at DOI: 10.1021/acs.jpcc.6b05930.

The FESEM image of pure nickel cobaltite nanostructure, BET analysis of pure nickel cobaltite and rGO/NCO, XRD diffractogram of rGO/NCO before and after thermal treatment, wide scan XPS spectrum of rGO/NCO, and the CV curves of pure nickel cobaltite electrode (PDF)

AUTHOR INFORMATION

Corresponding Author

*E-mail: janetlimhn@gmail.com. Tel.: +6016 330 1609.

Notes

The authors declare no competing financial interest.

ACKNOWLEDGMENTS

This research work was supported by Putra Grant IPB (GP-IPB/2014/9440701) from Universiti Putra Malaysia.

REFERENCES

(1) Bruce, P. G.; Freunberger, S. A.; Hardwick, L. J.; Tarascon, J. M. Li-O_2 and Li-S Batteries with High Energy Storage. *Nat. Mater.* **2012**, *11*, 19−29.

(2) Bruce, P. G.; Scrosati, B.; Tarascon, J. M. Nanomaterials for Rechargeable Lithium Batteries. *Angew. Chem., Int. Ed.* **2008**, *47*, 2930−2946.

(3) Ellis, B. L.; Nazar, L. F. Sodium and Sodium-Ion Energy Storage Batteries. *Curr. Opin. Solid State Mater. Sci.* **2012**, *16*, 168−177.

(4) Jossen, A.; Garche, J.; Doering, H.; Goetz, M.; Knaupp, W.; Joerissen, L. Hybrid Systems with Lead−Acid Battery and Proton-Exchange Membrane Fuel Cell. *J. Power Sources* **2005**, *144*, 395−401.

(5) Wang, Y.; Shi, Z.; Huang, Y.; Ma, Y.; Wang, C.; Chen, M.; Chen, Y. Supercapacitor Devices Based on Graphene Materials. *J. Phys. Chem. C* **2009**, *113*, 13103−13107.

(6) Zhang, L. L.; Zhao, X. S. Carbon-Based Materials as Supercapacitor Electrodes. *Chem. Soc. Rev.* **2009**, *38*, 2520−2531.

(7) Lee, Y. H.; Goodenough, J. B. Supercapacitor Behavior with KCl Electrolyte. *J. Solid State Chem.* **1999**, *144*, 220−223.

(8) Liu, C.; Yu, Z.; Neff, D.; Zhamu, A.; Jang, B. Z. Graphene-Based Supercapacitor with an Ultrahigh Energy Density. *Nano Lett.* **2010**, *10*, 4863−4868.

(9) Liu, Y.; Wang, R.; Yan, X. Synergistic Effect Between Ultra-Small Nickel Hydroxide Nanoparticles and Reduced Graphene Oxide Sheets for the Application in High-Performance Asymmetric Supercapacitor. *Sci. Rep.* **2015**, *5*, 11095.

(10) Futaba, D. N.; Hata, K.; Yamada, T.; Hiraoka, T.; Hayamizu, Y.; Kakudate, Y.; Tanaike, O.; Hatori, H.; Yumura, M.; Iijima, S. Shape-Engineerable and Highly Densely Packed Single-Walled Carbon Nanotubes and their Application as Super-Capacitor Electrodes. *Nat. Mater.* **2006**, *5*, 987−994.

(11) Wang, R.; Yan, X. Superior Asymmetric Supercapacitor Based on Ni-Co Oxide Nanosheets and Carbon Nanorods. *Sci. Rep.* **2014**, *4*, 3712.

(12) Zhang, K.; Zhang, L. L.; Zhao, X. S.; Wu, J. Graphene/Polyaniline Nanofiber Composites as Supercapacitor Electrodes. *Chem. Mater.* **2010**, *22*, 1392−1401.

(13) Yang, S.; Gong, Y.; Liu, Z.; Zhan, L.; Hashim, D. P.; Ma, L.; Vajtai, R.; Ajayan, P. M. Bottom-Up Approach Toward Single-Crystalline VO_2-Graphene Ribbons as Cathodes for Ultrafast Lithium Storage. *Nano Lett.* **2013**, *13*, 1596−1601.

(14) Dubal, D. P.; Gomez-Romero, P.; Sankapal, B. R.; Holze, R. Nickel Cobaltite as an Emerging Material for Supercapacitors: An Overview. *Nano Energy* **2015**, *11*, 377−399.

DOI: 10.1021/acs.jpcc.6b05930
J. Phys. Chem. C XXXX, XXX, XXX−XXX

(15) Cheng, J.; Lu, Y.; Qiu, K.; Yan, H.; Xu, J.; Han, L.; Liu, X.; Luo, J.; Kim, J. K.; Luo, Y. Hierarchical Core/Shell $NiCo_2O_4$@$NiCo_2O_4$ Nanocactus Arrays with Dual-Functionalities for High Performance Supercapacitors and Li-Ion Batteries. *Sci. Rep.* **2015**, *5*, 12099.
(16) Dubal, D. P.; Gund, G. S.; Lokhande, C. D.; Holze, R. Decoration of Spongelike $Ni(OH)_2$ Nanoparticles onto MWCNTS Using an Easily Manipulated Chemical Protocol for Supercapacitors. *ACS Appl. Mater. Interfaces* **2013**, *5*, 2446−2454.
(17) Adán-Más, A.; Wei, D. Photoelectrochemical Properties of Graphene and its Derivatives. *Nanomaterials* **2013**, *3*, 325−356.
(18) Johra, F. T.; Jung, W.-G. RGO−TiO_2−ZnO Composites: Synthesis, Characterization, and Application to Photocatalysis. *Appl. Catal., A* **2015**, *491*, 52−57.
(19) Gwon, H.; Kim, H. S.; Lee, K. U.; Seo, D. H.; Park, Y. C.; Lee, Y. S.; Ahn, B. T.; Kang, K. Flexible Energy Storage Devices Based on Graphene Paper. *Energy Environ. Sci.* **2011**, *4*, 1277.
(20) Pumera, M. Electrochemistry of Graphene: New Horizons for Sensing and Energy Storage. *Chem. Rec.* **2009**, *9*, 211−223.
(21) Pumera, M. Graphene-Based Nanomaterials for Energy Storage. *Energy Environ. Sci.* **2011**, *4*, 668−674.
(22) Wang, D.; Kou, R.; Choi, D.; Yang, Z.; Nie, Z.; Li, J.; Saraf, L. V.; Hu, D.; Zhang, J.; Graff, G. L.; Liu, J.; Pope, M. A.; Aksay, I. A.; et al. Ternary Self-Assembly of Ordered Metal Oxide-Graphene Nanocomposite for Electrochemical Energy Storage. *ACS Nano* **2010**, *4* (3), 1587−1595.
(23) Xu, J.; Wang, K.; Zu, S. Z.; Han, B. H.; Wei, Z. Hierarchical Nanocomposites of Polyaniline Nanowire Arrays on Graphene Oxide Sheets with Synergistic Effect for Energy Storage. *ACS Nano* **2010**, *4* (9), 5019−5026.
(24) Chen, S.; Zhu, J.; Wu, X.; Han, Q.; Wang, X. Graphene Oxide/MnO_2 Nanocomposite for Supercapacitor. *ACS Nano* **2010**, *4* (5), 2812−2830.
(25) Yao, J.; Shen, X.; Wang, B.; Liu, H.; Wang, G. In Situ Chemical Synthesis of SnO_2−Graphene Nanocomposite as Anode Materials for Lithium-Ion Batteries. *Electrochem. Commun.* **2009**, *11*, 1849−1852.
(26) Dembele, K. T.; Selopal, G. S.; Soldano, C.; Nechache, R.; Rimada, J. C.; Concina, I.; Sberveglieri, G.; Rosei, F.; Vomiero, A. Hybrid Carbon Nanotubes−TiO_2 Photoanodes for High Efficiency Dye-Sensitized Solar Cells. *J. Phys. Chem. C* **2013**, *117*, 14510−14517.
(27) Ma, H.; Tian, J.; Cui, L.; Liu, Y.; Bai, S.; Chen, H.; Shan, Z. Porous Activated Graphene Nanoplatelets Incorporated in TiO_2 Photoanodes for High-Efficiency Dye-Sensitized Solar Cells. *J. Mater. Chem. A* **2015**, *3*, 8890−8895.
(28) Cao, J.; Wang, Y.; Zhou, Y.; Ouyang, J.-H.; Jia, D.; Guo, L. Symmetric Supercapacitor Based on MnO_2 and Graphene Electrodes. *J. Electroanal. Chem.* **2013**, *689*, 201−206.
(29) Guo, C. X.; Li, C. M. A Self-Assembled Hierarchical Nanostructure Comprising Carbon Spheres and Graphene Nanosheets for Enhanced Supercapacitor Performance. *Energy Environ. Sci.* **2011**, *4*, 4504.
(30) Le, L. T.; Ervin, M. H.; Qiu, H.; Fuchs, B. E.; Lee, W. Y. Graphene Supercapacitor Electrodes Fabricated by Inkjet Printing and Thermal Reduction of Graphene Oxide. *Electrochem. Commun.* **2011**, *13*, 355−358.
(31) Yin, S.; Zhang, Y.; Kong, J.; Zou, C.; Li, C. M.; Lu, X.; Ma, J.; Boey, F. Y. C.; Chen, X. Assembly of Graphene Sheets into Hierarchical Structures for High-Performance Energy Storage. *ACS Nano* **2011**, *5*, 3831−3838.
(32) Fan, Z.; Yan, J.; Wei, T.; Zhi, L.; Ning, G.; Li, T.; Wei, F. Assymetric Supercapacitor Based on Graphene/MnO_2 and Activated Carbon Nanofibers Electrode with High Power and Energy Density. *Adv. Funct. Mater.* **2011**, *21*, 2366−2375.
(33) Huang, N. M.; Lim, H. N.; Chia, C. H.; Yarmo, M. A.; Muhamad, M. R. Simple Room-Temperature Preparation of High-Yield Large-Area Graphene Oxide. *Int. J. Nanomed.* **2011**, *6*, 3443−3448.
(34) Umeshbabu, E.; Rajeshkhanna, G.; Justin, P.; Rao, G. R. Synthesis of Mesoporous $NiCo_2O_4$−RGO by A Solvothermal Method for Charge Storage Applications. *RSC Adv.* **2015**, *5*, 66657−66666.
(35) Rusi; Majid, S. R. Green Synthesis Of In Situ Electrodeposited RGO/MnO_2 Nanocomposite for High Energy Density Supercapacitors. *Sci. Rep.* **2015**, *5*, 16195.
(36) Lee, E.; Lu, J.; Ren, Y.; Luo, X.; Zhang, X.; Wen, J.; Miller, D.; DeWahl, A.; Hackney, S.; Key, B.; Kim, D.; Slater, M. D.; Johnson, C. S. Layered P_2/O_3 Intergrowth Cathode: Toward High Power Na-Ion Batteries. *Adv. Energy Mater.* **2014**, *4*, 1400458.
(37) Syedvali, P.; Rajeshkhanna, G.; Umeshbabu, E.; Kiran, G. U.; Rao, G. R.; Justin, P. In Situ Fabrication of Graphene Decorated Microstructured Globe Artichokes of Partial Molar Nickel Cobaltite Anchored on a Ni Foam as a High-Performance Supercapacitor Electrode. *RSC Adv.* **2015**, *5*, 38407−38416.
(38) Garg, N.; Basu, M.; Ganguli, A. K. Nickel Cobaltite Nanostructures with Enhanced Supercapacitance Activity. *J. Phys. Chem. C* **2014**, *118*, 17332−17341.
(39) Guo, S.; Yu, H.; Liu, P.; Ren, Y.; Zhang, T.; Chen, M.; Ishida, M.; Zhou, H. High-Performance Symmetric Sodium-Ion Batteries Using a New, Bipolar O_3-Type Material, Na 0.8 Ni 0.4 Ti 0.6 O 2. *Energy Environ. Sci.* **2015**, *8*, 1237−1244.
(40) Liu, W.-w.; Lu, C.; Liang, K.; Tay, B. K. A Three Dimensional Vertically Aligned Multiwall Carbon Nanotube/$NiCo_2O_4$ Core/Shell Structure for Novel High-Performance Supercapacitors. *J. Mater. Chem. A* **2014**, *2*, 5100−5107.
(41) Wu, J.; Guo, P.; Mi, R.; Liu, X.; Zhang, H.; Mei, J.; Liu, H.; Lau, W.-M.; Liu, L.-M. Ultrathin $NiCo_2O_4$ Nanosheets Grown on Three-Dimensional Interwoven Nitrogen-Doped Carbon Nanotubes as Binder-Free Electrodes for High-Performance Supercapacitors. *J. Mater. Chem. A* **2015**, *3*, 15331−15338.

DOI: 10.1021/acs.jpcc.6b05930
J. Phys. Chem. C XXXX, XXX, XXX−XXX